MrSARP: A Hierarchical Deep Generative Prior for SAR Image Super-resolution

Tushar Agarwal, Nithin Sugavanam and Emre Ertin
Department of Electrical and Computer Engineering, The Ohio State University

***Abstract*—Generative models learned from training using deep learning methods can be used as priors in under-determined inverse problems, including imaging from sparse set of measurements. In this paper, we present a novel hierarchical deep-generative model MrSARP for SAR imagery that can synthesize SAR images of a target at different resolutions jointly. MrSARP is trained in conjunction with a critic that scores multi resolution images jointly to decide if they are realistic images of a target at different resolutions. We show how this deep generative model can be used to retrieve the high spatial resolution image from low resolution images of the same target. The cost function of the generator is modified to improve its capability to retrieve the input parameters for a given set of resolution images. We evaluate the model's performance using three standard error metrics used for evaluating super-resolution performance on simulated data and compare it to upsampling and sparsity based image super-resolution approaches.**

***Index Terms*—Deep Learning, Super-Resolution, Compressive sensing.**

I. Introduction

Synthetic aperture radar (SAR) imagery captures the physical aspects of the target differently compared to the optical imagery because of multi-path reflections, specular nature of reflectors, and imaging geometry effects leading to overlay as well as shadowing. Traditional approaches that utilize the sparsity in the image domain captures the effects of dominant reflectors that account for only the specular nature of reflectors [1], [2]. In this work, we present a data-driven generative model that captures several aspects of SAR phenomenology at different resolutions exhibited by SAR magnitude imagery. Specifically, we propose a specialized hierarchical architecture of the generative model, called MrSARP, that jointly models the data manifold of multiple-resolutions of a SAR image. We show that such a generative model acts as the projection operator to a lower dimensional manifold and can be directly used for super-resolving magnitude SAR images from low resolution magnitude images. The super-resolution performance of MrSARP is evaluated by comparing it with LASSO (or L_1 recovery) and Nearest Neighbor Upsampling using empirical data.

Next, we describe important notation used throughout the text. The lower-case character x represents a fixed sample value of a random vector (rv) X (the corresponding upper-case character), $M:N$ is the enumeration of natural numbers from M to N, $g(X_{1:N};w)$ denotes function g of rv's $X_{1:N}$ with deterministic parameters w and an index-based $x[v]$ represents the v^{th} value from the ordered set $\{x[i]:i\in\{1:N\}\}$. Formal definitions of terms Generative Modeling and Compressed Sensing, as used in the context of this paper, are stated below.

Definition 1 (Generative Modeling)**.** *Generative Modeling aims to estimate the distribution $p(X)$ using a parameterized distribution family $q(X;w)$ and a set $\mathcal{D}$ of samples from the distribution $p(X)$. The stochasticity in sampling is typically achieved by sampling a low-dimensional latent rv Z, internal to $q(X;w)$, from a simple distribution (e.g. standard gaussian). Therefore, the goal is to generate N realistic samples $\{\hat{X}[v]\}_{v=1}^{N}$ from $q(X;w)$ as if they were from $p(X)$.*

Definition 2 (Compressed Sensing)**.** *Given measurements $y\in\mathbb{C}^d$ obtained using a known measurement (or forward) operator F of an underlying signal $x\in\mathbb{C}^D$, Compressed Sensing seeks to recover this underlying signal under the model [3]*

$$y=F(x)+\eta,\qquad x\in\Omega, \tag{1}$$

where η is the measurement noise and Ω represents the constraint set that is non-convex. It is an under-determined system of equations, i.e., the no. of measurements are less than the signal dimension and so the signal structure must be exploited through appropriate constraints to obtain a unique solution for the problem [4]:

$$\min_{x\in\Omega}\qquad L(F(x);y) \tag{2}$$

Where $L(F(x);y)$ is an appropriate loss function to be minimized.

We want to use the range space of the generative model $q(X;w)$ as the constraint set Ω that can super-resolve SAR data as well as potentially be used to solve a compressed sensing problem for SAR data. Specifically, we want to find a prior function as an Artificial Neural Network (ANN) based generative model G with parameters w_G, that generates random samples of X (SAR magnitude images) using a low-dimensional latent rv Z, i.e. sampling from $G(Z;w_G)$ is a good approximation of sampling from $p(X)$. This implicitly constrains samples X on a low-dimensional manifold while having the flexibility to adapt the basis to any dataset, unlike commonly used sparsity priors. Therefore, G can be used as the learned projection function $\mathcal{P}_\Omega$ in a Projected Gradient Descent optimization to find the solution in the constraint set Ω. We show that a specially designed G can itself be used for super-resolving SAR images directly. The dataset of all sam-

ples is split into 3 subsets $\mathcal{D}_{train}$, $\mathcal{D}_{val}$ and $\mathcal{D}_{test}$ for model training, cross-validation and evaluation of G respectively.

A. Related Work

A survey of trained and untrained DL methods to solve the Inverse problems is given in [5]. Data-driven models can be broadly classified as end-to-end models that are agnostic to the measurement operator and deep generative priors that model the distribution representing the constraint set estimated from a corpus of data. We will discuss the approaches based on the latter briefly.

Theoretical guarantees are established on the number of measurements and conditions on the generator network for successful reconstruction in [6]. A generative model is estimated on a large corpus of natural images in [7]. Given the generator, which is implemented as a generative adversarial network or variational auto-encoder and the measurements, we can infer the image by solving (2). The projection operator $\mathcal{P}_\Omega$ for the set of natural images Ω is learned from a large corpus of data using an adversarial network in [8]. This projection operator is used in solving any inverse problem in a plug and play manner since the projection operator has enough capacity to model the complicated non-convex set of natural images. Theoretical guarantees for the generative prior are established in [9]. It is shown that if the entries of the generator function is near-random and the number of weights in each layer increases with the width then the loss function landscape contains descent directions to the global optima. The deep-geometric prior is extended to MR imaging in [10] where authors use invertible generators. Since the dimensionality of the latent code is large and equivalent to the signal dimension, a block-wise structure is imposed on the structure of the latent variable. The idea of generative prior is extended to video-sequences in a novel way to synthesize video from a sub-sample of image frames in [11]. The image sequences in time are denoted by $X = \mathbf{x}_1, \mathbf{x}_2, \cdots, \mathbf{x}_T$. It is shown that if all the images are obtained from the same generator, then the network parameters θ can be fixed and for each image in the sequence, a latent code can be estimated to succinctly represent the video. The latent code sequence $Z = [\mathbf{z}_1, \mathbf{z}_2, \cdots, \mathbf{z}_T]$ compactly represents the images. The smoothness in the image sequences of a video can be imposed by imposing a smoothness constraint or a low-rank constraint on the latent code Z while jointly estimating in the prediction step. Furthermore if images are dissimilar, then the network parameters θ can also be re-trained to capture the variability. It is shown that missing frames can be synthesized using interpolation in the latent space. Next, we consider the regime when no or limited training data is available, where the generator is estimated for each image.

Deep image prior [12] presents a non-trained version of the generator discussed in previous section. The latent code is assumed fixed and can be chosen arbitrarily but the network parameters are optimized to represent the image. It is hypothesized that the structure of the network imposes a strong regularizer or prior on the image. This strong prior is shown to have high impedance to noise and uncorrelated samples. Therefore, the optimization problem solved is

$$\min_{\theta} L(g(\mathbf{z}, \theta), \mathbf{y}, F). \tag{3}$$

The main problem is over-fitting and it is shown that early-stopping is necessary to capture the de-noised image. Various ANN architectures are explored and it is empirically shown that as the network is over-parameterized, the performance improves because the capacity of the network to learn the image is increased.

The works in [13], and [14] propose an alternative loss function termed as the backprojection loss and demonstrate the efficacy theoretically as well as empirically for multiple imaging linear inverse problems such as de-blurring and super-resolution as a function of the condition-number of the measurement operator. The loss function considered is

$$L(\theta) = \|F^{+}(\mathbf{y} - Fg(\mathbf{x}, \theta))\|^2, \tag{4}$$

where F^{+} denotes the pseudo-inverse of the linear measurement operator. Theoretical guarantees for compressive sensing are established for deep priors for [15], and [16]. It is shown that the number of measurements required are similar to the traditional requirements established in compressive sensing. Empirically, these methods are shown to perform better than ℓ_1 and TV norm regularization on fastMRI dataset.

II. Method

Building upon eq. 2, squared Euclidean L_2 norm is commonly used for the loss function, i.e., $L(F(x); y) = \|y - F(x)\|_2^2$ under the assumption that η is additive Gaussian noise. Sparsity in some known basis Φ, such as Fourier or Wavelet basis, is the most widely used constraint on x, achieved by adding L_1 regularization to sparse vector $\tilde{x}$ where $\tilde{x}$ is such that $x = \Phi\tilde{x}$. This derivation involves a convex relaxation as well as Φ must follow the restricted isometry property and [17] can be referred for details. Instead of this sparsity assumption, we follow a different approach. The problem in eq. 2 can also be solved by finding a convex relaxation of the constraint set Ω and using a projected gradient method as

$$\begin{aligned} \hat{x}_{mp} &= \arg\min_{x} \|y - F(x)\|_2^2 \\ &= \arg\min_{m,p} \|y - F(m \odot \exp(jp))\|_2^2 \end{aligned} \tag{5}$$

$$\hat{x}_\Omega = \mathcal{P}_\Omega(\hat{x}_{mp}) = \arg\min_{x \in \Omega} \|\hat{x}_{mp} - x\|_2^2 \tag{6}$$

Where m, p are magnitude and phase of complex-valued x respectively alongwith subscripts (if any), $\mathcal{P}_\Omega$ denotes the projection operator onto set Ω Alternating between these two steps will find the desired solution if Ω and F were convex starting from an appropriate initial condition x_0. However, like most signals of interest x, we don't know Ω for SAR data. Therefore, similar to Projected Gradient Descent GAN by Shah and Hegde [18], we propose to learn Ω as the range-space of an ANN based Generative model $G(Z; w_G)$. Here, Z as much lower dimensionality than x. Moreover, we only constrain the magnitude m of x using $G(Z; w_G)$ and allow

phase p to be unconstrained without projection. Assuming that we have obtained such a $G(Z; w_G)$ that well approximates the probability distribution $P(m)$, projection $\hat{x}_\Omega$ becomes

$$\begin{aligned}\hat{x}_\Omega &= \mathcal{P}_\Omega(\hat{m}_{mp} \odot \exp(j\hat{p}_{mp})) \quad = \mathcal{P}_G(\hat{m}_{mp}) \odot \exp(j\hat{p}_{mp}) \\ &= \hat{m}_G \odot \exp(j\hat{p}_{mp}) \end{aligned} \tag{7}$$

Where $\hat{m}_G$ is the projection of magnitude $\hat{m}_{mp}$ derived using G. Here, the magnitude m of the structured signal x is assumed to be sampled from a low-dimensional manifold with a latent variable z. To find $\hat{m}_G$, we first optimize over z starting from initial condition $z_0 = 0$ as

$$z_z^* = \arg\min_z \|\hat{m}_{mp} - G(z; w_G)\|_2^2 \tag{8}$$

However, since G is a non-linear ANN, range-space of $G(Z; w_G)$ is non-convex. Therefore, solving optimization problem in eq. 8 only guarantees local-minima. Hence, it will be sensitive to initialization and may yield inconsistent projections. Motivated from works of Bojanowski et al. [19] and Wu et al. [20], we attempt to alleviate this problem by making $G(Z; w_G)$ aware of this inversion task during its training phase. This is described in section III.

Additionally, we borrow important ideas from similar work of IAGAN [21]. Even after significant progress in Deep Generative Modeling, such models are still an approximation of the true distribution due to limited representation capabilities of ANN. Therefore, magnitudes m of many samples x may not even belong to the range-space of $G(Z; w_G)$. To mitigate this, IAGAN proposes to do image-adaptive projections, i.e. optimizing over both latent vector z and ANN weights w when projecting. This adds the following step to eq. 8 as

$$(z_{zw}^*, w_G^*) = \arg\min_{z,w} \|\hat{m}_{mp} - G(z; w)\|_2^2 \tag{9}$$

Where z, w are initialized as $z_0 = z_z^*$, $w_0 = w_G$ respectively while optimizing eq. 9. Finally, the magnitude projection required for eq. 7 is $\hat{m}_G = \mathcal{P}_G(\hat{m}_{mp}) = G(z_{zw}^*; w_G^*)$. We call our complete algorithm as Image Adaptive Projected Gradient Descent WGAN and it is mentioned in algorithm 1.

Algorithm 1 IAPGD WGAN

Require: $n, n_{mp}, n_z, n_{zw} \geq 0, y, F, G(z; w_G), x_0$

1: **while** $n \neq 0$ **do**
2: $\quad \hat{x}_{mp} \leftarrow \left[\arg\min_{m,p} \|y - F(m \odot \exp(jp))\|_2^2\right]_{n_{mp}}$
3: $\quad \hat{m}_{mp} \leftarrow |\hat{x}_{mp}|$
4: $\quad z_0 \leftarrow 0$
5: $\quad z_z^* \leftarrow \left[\arg\min_z \|\hat{m}_{mp} - G(z; w_G)\|_2^2\right]_{n_z}$
6: $\quad (z_0, w_0) \leftarrow (z_z^*, w_G)$
7: $\quad (z_{zw}^*, w_G^*) \leftarrow \left[\arg\min_{z,w} \|\hat{m}_{mp} - G(z; w)\|_2^2\right]_{n_{zw}}$
8: $\quad \hat{m}_G \leftarrow G(z_{zw}^*; w_G^*)$
9: $\quad \hat{x}_\Omega \leftarrow \hat{m}_G \odot \exp(j\hat{p}_{mp})$
10: $\quad x_0 \leftarrow \hat{x}_\Omega$
11: $\quad n \leftarrow n - 1$
12: **end while**

Where the notation $[\arg\min_x \mathcal{L}(x)]_{n_x}$ refers to minimizing the loss $\mathcal{L}(x)$ for n_x steps iteratively using a variant of Stochastic Gradient Descent (SGD).

We propose a special hierarchical architecture of a WGAN that jointly generates magnitude of multiple resolutions of the same SAR image. This idea of jointly modeling multiple resolutions was inspired from the Progressive GAN by Karras et al. [22] though their motivations were different. We aim to exploit this hierarchical structure for super-resolution i.e. to find a higher resolution image given its lower resolutions. Suppose we are given a dataset containing 4 exponentially increasing resolution images' magnitude $m^{r_1}, m^{r_2}, m^{r_3}, m^{r_4}$ where resolution of $m^{r_{i+1}}$ is twice of m^{r_i}. Then our WGAN $G(Z; w_G)$ models the joint probability distribution $P(m^{r_1}, m^{r_2}, m^{r_3}, m^{r_4})$. Now if we are given a new sample from $P(m^{r_1}, m^{r_2}, m^{r_3})$ i.e. of the 3 lower resolutions, we can use $G(Z; w_G)$ and steps 4 to 8 of algorithm 1 to project it onto the joint data manifold of $P(m^{r_1}, m^{r_2}, m^{r_3}, m^{r_4})$ by finding a common (z_{zw}^*, w_G^*) pair. The highest resolution r_4 image is then obtained by a simple forward pass $\hat{m}_G^{r_4} = G(z_{zw}^*, w_G^*)$. The overall algorithm is therefore Projecting from a Multi-Resolution SAR Prior (or MrSARP) and is summarized in algorithm 2. Note that $G(z; w_G)^{r_i}$ denotes r_i resolution output from $G(z; w_G)$ and $G(z; w_G)^{r_4}$ is simply dropped in step 2.

Algorithm 2 Projecting from MrSARP

Require: $n_z, n_{zw} \geq 0, m^{r_1}, m^{r_2}, m^{r_3}, G(z; w_G)$

1: $z_0 \leftarrow 0$
2: $z_z^* \leftarrow \left[\arg\min_z \Sigma_{i=1}^3 \|m^{r_i} - G(z; w_G)^{r_i}\|_2^2\right]_{n_z}$
3: $(z_0, w_0) \leftarrow (z_z^*, w_G)$
4: $(z_{zw}^*, w_G^*) \leftarrow \left[\arg\min_{z,w} \Sigma_{i=1}^3 \|m^{r_i} - G(z; w)^{r_i}\|_2^2\right]_{n_{zw}}$
5: $\hat{m}_G^{r_4} \leftarrow G(z_{zw}^*; w_G^*)^{r_4}$

III. Model

MrSARP consists of a WGAN-GP [23] with a Hierarchical architecture. Our architecture is inspired from the CIFAR-10 ResNet architecture used by Gulrajani et al. [23] and ProGAN [22]. We use the ResNet block from the former and the idea of FromImage/ToImage layers at various ResNet input/output features from latter. The schematic of the hierarchical model is shown in figure 1. The output shapes of layers are specified. The ResNet blocks in the generator use Batch-Normalization layers and have nearest-neighbour upsampling after the input. The ResNet blocks in the critic uses Layer-Normalization layers and have an average pooling based downsampling before the final output, and channel-wise concatenation in case of multiple inputs. The FromImage layer is a 2D convolution layer with 1 channel input (image) and 2 channel output (features). The ToImage layer comprises slicing first 2 channels of input features, Batch-Normalization, ReLU activation and 2D convolution layer with 1 channel output (image) after tanh activation. All convolutional layers in the generator have kernel-size as 3 and ReLU activation function. All convolutional layers in the critic have kernel-size as 3 and LeakyReLU activation function with 0.2 slope.

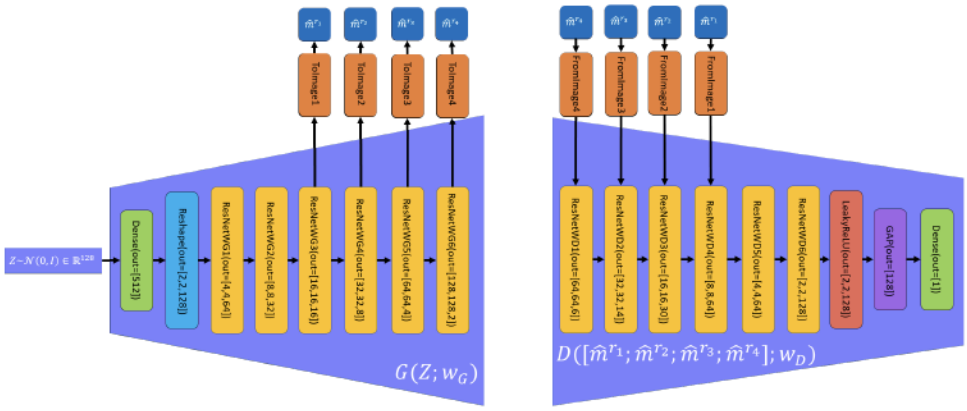

(a) Generator (b) Critic

Fig. 1: Hierarchical Model Architecture of MrSARP

The dense (or fully-connected) layers in both, generator and critic have linear activation and the GAP referes to Global Average Pooling operation. The generator $G(Z; w_G)$ of MrSARP generates samples from the unconditional joint distribution of 4 resolutions of SAR images $P(m^{r_1}, m^{r_2}, m^{r_3}, m^{r_4})$ where resolution of m_{r_i} is $2^{i+3} \times 2^{i+3}$ and bandwidth is $125.2^i Mhz$..

WGAN-GP was chosen because of its advantages over traditional GANs, especially meaningful loss curves for cross-validation and reliable training as demonstrated by Gulrajani et al. [23]. WGAN-GP, like all GANs, require an extra critic ANN $D(\cdot, \cdot; w_D)$ to be learned simultaneously to aid the learning of the generator. Both, the critic and generator are trained alternately using gradient descent steps. Latent variable $Z \sim \mathcal{N}(0, I)$ as in a conventional GAN.

Since MrSARP would primarily be used for inverting and projecting on data-manifold instead of sampling, we think it is essential to inform the generator G about this task during training. Inspired from Wu et al's work [20], we add Model Agnostic Meta Learning (MAML) based regularizing loss term to the overall loss functions used for training G. Proposed by Finn et al. [24], MAML is a general-purpose meta-learning method to adapt parameters w of a statistical model to a number of tasks as long as the loss function $\mathcal{L}(\mathcal{T}; w)$ for the task $\mathcal{T}$ is differentiable. Since our primary task is inversion using step 2 of algorithm 2, we perform a small number $n_z = 5$ iterations of this optimization step to get z^* and use residual error on all 4 channels as our MAML loss $\mathcal{L}_{MAML}$. Since the $Z \sim \mathcal{N}(0, I)$ with high dimensionality d_Z, the samples lie near the hypersphere of $\sqrt{d_Z}$. To enforce such a constraint on z^*, we additionally project z^* on to the $\sqrt{d_Z}$ hypersphere after every SGD step using projection operator $\mathcal{P}_{\mathcal{S}}$. The complete loss functions are as follows.

$$\mathcal{L} = \begin{cases} -\mathcal{L}_W + \lambda_1 \mathcal{L}_{GP} & \text{for } D \\ \mathcal{L}_W + \lambda_2 \mathcal{L}_{MAML} & \text{for } G \end{cases} \tag{10}$$

$$\mathcal{L}_W = \mathbb{E}_m \left[D(m); w_D \right] - \mathbb{E}_Z \left[D(G(Z; w_G); w_D) \right]$$

$$\mathcal{L}_{GP} = \mathbb{E}_{\bar{m}} (\|\nabla_{\bar{m}} D(\bar{m}; w_D)\|_2 - 1)^2$$

$$\mathcal{P}_{\mathcal{S}}(z^*) = \frac{z^*}{\min(\|z^*\|_2, \sqrt{d_Z})} \cdot \sqrt{d_Z} \tag{11}$$

$$z_S^* = \left[\mathcal{P}_{\mathcal{S}} \left(\arg\min_z \Sigma_{i=1}^3 \|m^{r_i} - G(z; w_G)^{r_i}\|_2^2 \right) \right] \tag{12}$$

$$\mathcal{L}_{MAML} = \mathbb{E}_m \left[\Sigma_{i=1}^4 \|m^{r_i} - G(z_S^*; w_G)^{r_i}\|_2^2 \right] \tag{13}$$

Where $m \sim P(m^{r_1}, m^{r_2}, m^{r_3}, m^{r_4})$, $\bar{m} \sim r(\bar{M})$ is uniform-sampling along straight lines between pairs of sampled points m, $G(z; w_G)$. All expectations are approximated using corresponding empirical means. Motivated by [23], we employ negative critic loss as our primary metric for model selection. Hence, the weights of the final model are set to their values corresponding to the epoch where the smallest negative critic loss on $\mathcal{D}_{val}$ was achieved. For the hyperparameters, we use $\lambda_1 = 10$ (as in [23]) and set $\lambda_2 = 1000$ to approximately balance the two regularizing loss term L_{MAML} with the WGAN loss term $\mathcal{L}_W$ in magnitude.

IV. Experimental Setup

We use the Tensorflow (2.1) [25] deep-learning Python library for our ANN implementations. Unless mentioned otherwise, the Adam optimizer from Tensorflow with default parameters is used for most optimizations. We use NVIDIA GeForce RTX 2080 Ti GPU alongwith Intel Xeon CPU as our primary computation hardware.

A. CVDomes Dataset

We use the phase histories obtained from simulation of back-scattered energy from civilian vehicles in [26]. We consider only the HH polarization measurement in our experiment. The image at a bandwidth B and azimuth span $\Delta\theta$ is obtained by backprojection method using a Hamming window to suppress the side-lobes. We spotlight on a square patch of $9m \times 9m$. To generate 4 different resolutions $r1 : 4$, we repeat this process for 4 bandwidths 125.2^i and corresponding pixel resolutions $2^{i+3} \times 2^{i+3}$ for $i \in 1, 2, 3, 4$.

B. Pre-Processing

We work with magnitude images only for MrSARP. Hence, we first find the absolute values of complex-valued SAR images and then perform min-max normalization of every image individually to restrict their values in range $[-1, 1]$. We then upsample all lower resolution images to the highest resolution of 128×128 with nearest-neighbor upsampling and combine all 4 resolutions into a single 4 channel image. The lower resolution images are appropriately downsampled using average pooling before their input into the critic. This is only done to simplify multi-resolution architecture implementation and is based on the simple fact that nearest-neighbor upsampling followed by average-pooling gives identity function.

V. Results

We present some results of this study in this section. After training generator G as described in section III above, we use algorithm 2 to find the super-resolved images $\hat{m}_G^{r_4}$ for the unseen lower resolution samples in $\mathcal{D}_{test}$. We compare these images with the available ground truth images m^{r_4} qualitatively as well as using three quantitative metrics viz. PSNR (Peak Signal-to-Noise Ratio), NMSE (Normalised Mean Squared Error) as defined in [27] and SSIM (Structural Similarity Index) proposed in [28]. The use of these metrics is motivated from the evaluation schemes used in existing literature on super-resolution of SAR images e.g. [29]. These metric used are defined as follows.

$$MSE = \frac{1}{N_m} \|m^{r_4} - \hat{m}^{r_4}\|_F^2$$

$$PSNR = 10 \log_{10} \left(\frac{(\max(m^{r_4}) - \min(m^{r_4}))^2}{MSE} \right) \quad (14)$$

$$NMSE = \frac{\|m^{r_4} - \hat{m}^{r_4}\|_F^2}{\|m^{r_4}\|_F^2} \quad (15)$$

$$SSIM = l(x,y).c(x,y).s(x,y) \quad (16)$$

$$l(x,y) = \left(\frac{2\mu_x\mu_y + C_1}{\mu_x^2 + \mu_y^2 + C_1} \right)$$

$$c(x,y) = \left(\frac{2\sigma_x\sigma_y + C_2}{\sigma_x^2 + \sigma_y^2 + C_2} \right)$$

$$s(x,y) = \left(\frac{\sigma_{xy} + C_3}{\sigma_x\sigma_y + C_3} \right)$$

where N_m are total number of pixels in image m^{r_4}, μ_x, μ_y are empirical means of patches x, y respectively, σ_x, σ_y are sample standard deviations of patches x, y respectively, σ_{xy} is sample cross-correlation of x, y after mean subtraction and $C_{1:3}$ are small constants added for numerical stability. SSIM is calculated on smaller local patches x, y of size 7×7 and the mean SSIM is calculated for every image comparison pair $m^{r_4}, \hat{m}^{r_4}$. We also compare r_4 resolution estimate $\hat{m}_N^{r_4}$ obtained from nearest neighbor upsampling of m^{r_3} and estimates $\hat{m}_L^{r_4}$ obtained from using the popular LASSO method. The LASSO method is used to obtain the sparse scattering center representation of the vehicle at the resolution r_3. The sparse representation is projected back into the phase history measurement domain using the SAR forward operator. These measurements are converted to SAR imagery using the backprojection method with the hamming window at resolution r_4. All the evaluations are done on 504 images from the unseen $\mathcal{D}_{test}$.

TABLE I: Quantitative evaluation of Super-resolution performance.

Method	$NMSE \downarrow$	$PSNR \uparrow$	$SSIM \uparrow$
Nearest-Neighbor Upsampling	9.071	27.27	0.931
L_1 recovery	8.698	27.638	**0.937**
MrSARP	6.92	29.785	0.9
Image-Adaptive MrSARP	**6.003**	**30.963**	0.918

Figure 2 shows some samples from $\mathcal{D}_{test}$ that are super-resolved using different methods. There is a qualitative similarity between the Nearest Neighbor upsampled and L_1 recovered images. Both methods differ significantly from resulting images of MrSARP. The corresponding quantitative results are presented in table I. Addition of Image-Adaptive steps to MrSARP improves performance quantitatively for all 3 metrics. In fact, among all the methods tested, Image-Adaptive MrSARP results perform best in terms of both, $NMSE$ and $PSNR$. However, they are inferior to both Nearest Neighbor Upsampling and L_1 recovery in terms of SSIM indicating potential bias in amplitude for MrSARP.

VI. Conclusion

In this paper, we showed how a GAN with hierarchical architecture can jointly model the distribution of multiple resolutions of magnitude SAR images. We further showed how this GAN, called MrSARP, be used to for super-resolving SAR images. We saw some improvements over baselines of nearest neighbor upsampling as well as L_1 recovery in terms of $NMSE$ and $PSNR$ values but there is significant scope of further improvements in terms of perceptual quality. This was indicated by MrSARP's inferior performance in terms of SSIM. Furthermore, we plan to utilize this generative model and the proposed algorithm 1 to regularize inverse problems in SAR imaging with structured interrupted measurements.

Acknowledgements

This research was partially supported by NSF grants CNS-1823070 CBET-2037398 and NIH Grant P41EB028242

References

[1] N. Sugavanam, E. Ertin, and R. Burkholder, "Approximating bistatic sar target signatures with sparse limited persistence scattering models," in *Int. Conf. on Radar, Brisbane*, 2018.

[2] N. Sugavanam and E. Ertin, "Models of anisotropic scattering for 3d sar reconstruction," in *2022 IEEE Radar Conference (RadarConf22)*. IEEE, 2022, pp. 1–6.

[3] N. Sugavanam, E. Ertin, and R. Burkholder, "Compressing bistatic sar target signatures with sparse-limited persistence scattering models," *IET Radar, Sonar & Navigation*, vol. 13, no. 9, pp. 1411–1420, 2019.

[4] N. Sugavanam, S. Baskar, and E. Ertin, "High resolution mimo radar sensing with compressive illuminations," *IEEE Transactions on Signal Processing*, vol. 70, pp. 1448–1463, 2022.

[5] G. Ongie, A. Jalal, C. A. M. R. G. Baraniuk, A. G. Dimakis, and R. Willett, "Deep learning techniques for inverse problems in imaging," *IEEE Journal on Selected Areas in Information Theory*, 2020.

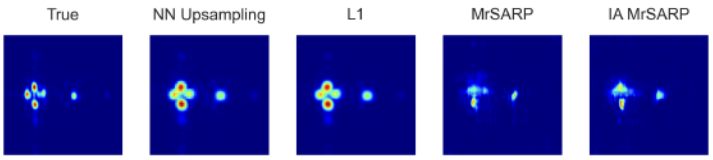

(a) Image 1

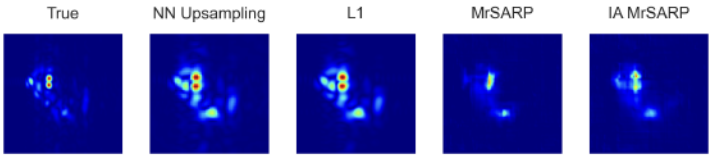

(b) Image 2

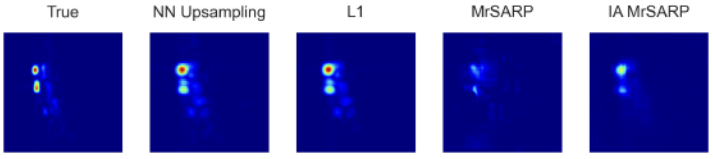

(c) Image 3

Fig. 2: Qualitative comparison of samples super-resolved using different methods

[6] Z. Liu and J. Scarlett, "Information-theoretic lower bounds for compressive sensing with generative models," *IEEE Journal on Selected Areas in Information Theory*, 2020.

[7] A. Bora, A. Jalal, E. Price, and A. G. Dimakis, "Compressed sensing using generative models," in *International Conference on Machine Learning*, 2017, pp. 537–546.

[8] J. H. R. Chang, C. Li, B. Póczos, B. V. K. Vijaya Kumar, and A. C. Sankaranarayanan, "One network to solve them all — Solving linear inverse problems using deep projection models," in *2017 IEEE International Conference on Computer Vision (ICCV)*, 2017, pp. 5889–5898.

[9] P. Hand and V. Voroninski, "Global guarantees for enforcing deep generative priors by empirical risk," *IEEE Transactions on Information Theory*, vol. 66, no. 1, pp. 401–418, 2019.

[10] V. A. Kelkar, S. Bhadra, and M. A. Anastasio, "Compressible latent-space invertible networks for generative model-constrained image reconstruction," *arXiv preprint arXiv:2007.02462*, 2020.

[11] R. Hyder and M. S. Asif, "Generative models for low-dimensional video representation and reconstruction," *IEEE Transactions on Signal Processing*, vol. 68, pp. 1688–1701, 2020.

[12] V. Lempitsky, A. Vedaldi, and D. Ulyanov, "Deep image prior," in *2018 IEEE/CVF Conference on Computer Vision and Pattern Recognition*, 2018, pp. 9446–9454.

[13] T. Tirer and R. Giryes, "Back-projection based fidelity term for ill-posed linear inverse problems," *IEEE Transactions on Image Processing*, vol. 29, pp. 6164–6179, 2020.

[14] J. Zukerman, T. Tirer, and R. Giryes, "BP-DIP: A backprojection based deep image prior," *arXiv preprint arXiv:2003.05417*, 2020.

[15] R. Heckel and M. Soltanolkotabi, "Compressive sensing with un-trained neural networks: Gradient descent finds the smoothest approximation," *arXiv preprint arXiv:2005.03991*, 2020.

[16] R. Heckel, "Regularizing linear inverse problems with convolutional neural networks," *arXiv preprint arXiv:1907.03100*, 2019.

[17] R. G. Baraniuk, V. Cevher, M. F. Duarte, and C. Hegde, "Model-Based Compressive Sensing," *IEEE Transactions on Information Theory*, vol. 56, no. 4, pp. 1982–2001, Apr. 2010. [Online]. Available: http://arxiv.org/abs/0808.3572

[18] V. Shah and C. Hegde, "Solving Linear Inverse Problems Using Gan Priors: An Algorithm with Provable Guarantees," in *2018 IEEE International Conference on Acoustics, Speech and Signal Processing (ICASSP)*, Apr. 2018, pp. 4609–4613.

[19] P. Bojanowski, A. Joulin, D. Lopez-Paz, and A. Szlam, "Optimizing the Latent Space of Generative Networks," May 2019. [Online]. Available: http://arxiv.org/abs/1707.05776

[20] Y. Wu, M. Rosca, and T. Lillicrap, "Deep Compressed Sensing," May 2019. [Online]. Available: http://arxiv.org/abs/1905.06723

[21] S. A. Hussein, T. Tirer, and R. Giryes, "Image-Adaptive GAN based Reconstruction," Nov. 2019. [Online]. Available: http://arxiv.org/abs/1906.05284

[22] T. Karras, T. Aila, S. Laine, and J. Lehtinen, "Progressive Growing of GANs for Improved Quality, Stability, and Variation," Feb. 2018. [Online]. Available: http://arxiv.org/abs/1710.10196

[23] I. Gulrajani, F. Ahmed, M. Arjovsky, V. Dumoulin, and A. Courville, "Improved Training of Wasserstein GANs," *arXiv:1704.00028 [cs, stat]*, Dec. 2017. [Online]. Available: http://arxiv.org/abs/1704.00028

[24] C. Finn, P. Abbeel, and S. Levine, "Model-Agnostic Meta-Learning for Fast Adaptation of Deep Networks," *arXiv:1703.03400 [cs]*, Jul. 2017. [Online]. Available: http://arxiv.org/abs/1703.03400

[25] M. Abadi, P. Barham, J. Chen, Z. Chen, A. Davis, J. Dean, M. Devin, S. Ghemawat, G. Irving, M. Isard, M. Kudlur, J. Levenberg, R. Monga, S. Moore, D. G. Murray, B. Steiner, P. Tucker, V. Vasudevan, P. Warden, M. Wicke, Y. Yu, and X. Zheng, "{TensorFlow}: A System for {Large-Scale} Machine Learning," in *12th USENIX Symposium on Operating Systems Design and Implementation (OSDI 16)*, 2016, pp. 265–283. [Online]. Available: https://www.usenix.org/conference/osdi16/technical-sessions/presentation/abadi

[26] K. E. Dungan, C. Austin, J. Nehrbass, and L. C. Potter, "Civilian vehicle radar data domes," in *Algorithms for Synthetic Aperture Radar Imagery XVII*, vol. 7699. SPIE, Apr. 2010, pp. 242–253. [Online]. Available: http://www.spiedigitallibrary.org/conference-proceedings-of-spie/7699/76990P/Civilian-vehicle-radar-data-domes/10.1117/12.850151.full

[27] N. Karimi and M. R. Taban, "Nonparametric blind SAR image super resolution based on combination of the compressive sensing and sparse priors," *Journal of Visual Communication and Image Representation*, vol. 55, pp. 853–865, 2018.

[28] Z. Wang, A. Bovik, H. Sheikh, and E. Simoncelli, "Image quality assessment: From error visibility to structural similarity," *IEEE Transactions on Image Processing*, vol. 13, no. 4, pp. 600–612, Apr. 2004.

[29] C. He, L. Liu, L. Xu, M. Liu, and M. Liao, "Learning Based Compressed Sensing for SAR Image Super-Resolution," *IEEE Journal of Selected Topics in Applied Earth Observations and Remote Sensing*, vol. 5, no. 4, pp. 1272–1281, Aug. 2012.